2012

Impact of Abrupt Deglacial Climate Change on Tropical Atlantic Subsurface Temperatures

Matthew W. Schmidt
Old Dominion University, mwschmid@odu.edu

Ping Chang

Jennifer E. Hertzberg

Theodore R. Them II

Link Li

See next page for additional authors

Original Publication Citation

Schmidt, M. W., Chang, P., Hertzberg, J. E., Them, T. R., Link, J., & Otto-Bliesner, B. L. (2012). Impact of abrupt deglacial climate change on tropical Atlantic subsurface temperatures. *Proceedings of the National Academy of Sciences of the United States of America, 109*(36), 14348-14352. doi:10.1073/pnas.1207806109

Impact of abrupt deglacial climate change on tropical Atlantic subsurface temperatures

Matthew W. Schmidt[a,1], Ping Chang[a,b], Jennifer E. Hertzberg[a], Theodore R. Them II[a], Link Ji[a], and Bette L. Otto-Bliesner[c]

[a]Department of Oceanography, Texas A&M University, College Station, TX 77843; [b]Physical Oceanography Laboratory, Ocean University of China, Qingdao 266003, People's Republic of China; and [c]National Center for Atmospheric Research, Boulder, CO 80307

Edited by James C. McWilliams, UCLA, Los Angeles, CA, and approved August 1, 2012 (received for review May 8, 2012)

Both instrumental data analyses and coupled ocean-atmosphere models indicate that Atlantic meridional overturning circulation (AMOC) variability is tightly linked to abrupt tropical North Atlantic (TNA) climate change through both atmospheric and oceanic processes. Although a slowdown of AMOC results in an atmospheric-induced surface cooling in the entire TNA, the subsurface experiences an even larger warming because of rapid reorganizations of ocean circulation patterns at intermediate water depths. Here, we reconstruct high-resolution temperature records using oxygen isotope values and Mg/Ca ratios in both surface- and subthermocline-dwelling planktonic foraminifera from a sediment core located in the TNA over the last 22 ky. Our results show significant changes in the vertical thermal gradient of the upper water column, with the warmest subsurface temperatures of the last deglacial transition corresponding to the onset of the Younger Dryas. Furthermore, we present new analyses of a climate model simulation forced with freshwater discharge into the North Atlantic under Last Glacial Maximum forcings and boundary conditions that reveal a maximum subsurface warming in the vicinity of the core site and a vertical thermal gradient change at the onset of AMOC weakening, consistent with the reconstructed record. Together, our proxy reconstructions and modeling results provide convincing evidence for a subsurface oceanic teleconnection linking high-latitude North Atlantic climate to the tropical Atlantic during periods of reduced AMOC across the last deglacial transition.

Mg/Ca paleothermometry | paleoclimate modeling | Bonaire Basin | Heinrich Event | sea surface temperature

Observational records of 20th century ocean-temperature variability in the tropical North Atlantic (TNA) show a strong anticorrelation between surface cooling and subsurface warming over the past several decades that is thought to be associated with recent variability in Atlantic meridional overturning circulation (AMOC) (1). Furthermore, coupled atmosphere-ocean general circulation model (AOGCM) simulations indicate that AMOC changes are tightly coupled to tropical Atlantic climate (2–6), revealing a prominent subsurface warming in the TNA resulting from a major reorganization of intermediate-water circulation in response to AMOC weakening (3, 7, 8). The subsurface warming and associated change in the vertical thermal gradient in the western TNA have been identified as an important fingerprint of AMOC variations (1). However, the validity of the modeling results during past abrupt climate events, when AMOC was significantly weakened, has not been fully tested because of a lack of high-resolution paleoproxy subsurface records. Most proxy reconstructions in the TNA are for sea surface temperature (SST), and these records tell an inconsistent story: Some indicate a surface cooling during the Younger Dryas (YD) cold period (9, 10) whereas others suggest SSTs increased (11–13). The only existing deglacial proxy records of intermediate-water change in the western TNA are a benthic foraminiferal $\delta^{18}O$ record from the Tobago Basin at approximately 1.3 km depth (14) and a benthic foraminiferal Mg/Ca record from the Florida Straits at approximately 750 m depth (15). Because observational and modeling studies point to the subsurface between 300 and 600 m depth in the western TNA as the region most sensitive to AMOC variability (2), there is a dire need for high-resolution subsurface proxy records of temperature change within this depth range.

To reconstruct vertical changes in the thermal gradient of the TNA upper-water column over the past 22 ky, we measure $\delta^{18}O$ values and Mg/Ca ratios (as temperature proxies) in the planktonic foraminifera *Globigerinoides ruber* and *Globorotalia crassaformis* from southern Caribbean sediment core VM12-107. Located between the Cariaco Basin and the Netherlands Antilles (Fig. S1), the core site is within a region influenced by coastal upwelling in the Bonaire Basin (Fig. 1).

Results

The age model for VM12-107 is based on 10 calibrated radiocarbon dates from planktonic foraminifera spanning the upper 270 cm of VM12-107, resulting in a deglacial sedimentation rate of approximately 18 cm/ky (Table 1 and Fig. S2). Radiocarbon ages were converted to calendar ages using CALIB 6.0 (16), using the standard 400–y reservoir age correction. Although recent studies suggest reservoir ages in the nearby Cariaco Basin may have varied by several hundred years during periods of AMOC slowdown, such as the start of the YD and Heinrich Event 1 (H1) (17–19), it is possible that these changes were a local effect within the basin caused by restricted circulation during periods of lower sea level (18) and that reservoir age changes in the open Caribbean/tropical Atlantic were much less. Furthermore, evidence suggests that deglacial reservoir age changes in the tropical Atlantic were restricted to only brief periods at the beginning of the YD, between 13.0 and 12.53 ky (17), and during H1 (18). Omission of the early YD radiocarbon date at 130 cm in the VM12-107 age model (calibrated age of 12.67 ky) only changes the timing of the start of the YD in the VM12-107 record by approximately 100 y (Figs. S2 and S3) and does not change the interpretation of the results.

G. ruber lives in the upper mixed layer in the southern Caribbean (20, 21). Although the life cycle of deep-dwelling planktonic foraminifera can involve a vertical migration of several hundred meters, *G. crassaformis* shell geochemistry indicates it mainly calcifies below the thermocline at a depth of 400–600 m in the southern Caribbean (20, 21). Based on shell oxygen isotope data, recent studies on the deep-dwelling planktonic foraminifera *G. crassaformis* and *Globorotalia truncatulinoides* from the Florida Straits and the Gulf of Mexico showed that, although *G. truncatulinoides* may have migrated to much shallower water depths

Author contributions: M.W.S. and P.C. designed research; M.W.S., P.C., J.E.H., and T.R.T. performed research; B.L.O.-B. contributed new reagents/analytic tools; M.W.S., P.C., J.E.H., T.R.T., and L.J. analyzed data; and M.W.S., and P.C., wrote the paper.

The authors declare no conflict of interest.

This article is a PNAS Direct Submission.

Data deposition: The data reported in this paper is archived at the National Oceanic and Atmospheric Administration Paleoclimatology database, www.ncdc.noaa.gov/paleo/paleo.html.

[1]To whom correspondence should be addressed. E-mail: schmidt@ocean.tamu.edu.

This article contains supporting information online at www.pnas.org/lookup/suppl/doi:10.1073/pnas.1207806109/-/DCSupplemental.

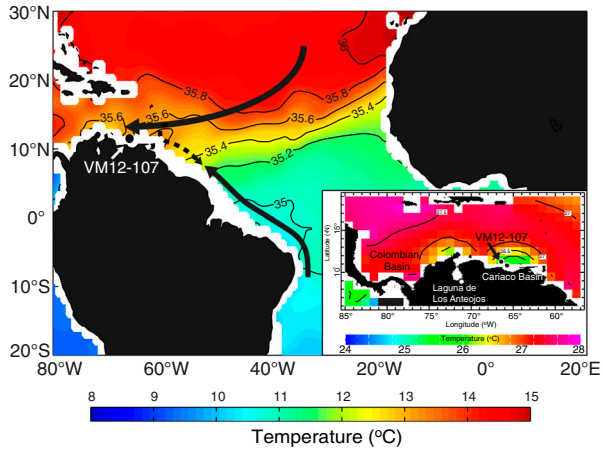

Fig. 1. Site location and modern surface and subsurface hydrography. Temperature (color) and salinity (contour) along density surface $\sigma = 1{,}026.8$ that varies from approximately 200 m near the equator to approximately 600 m in the subtropics. The sharp subsurface temperature gradient along the boundary between the subtropical and tropical gyres is evident, separating the warm SMW in the subtropical North Atlantic from the fresher tropical gyre water. This maximum subsurface temperature gradient forms at approximately 300 m, extending to the western boundary and intersecting with it near 10 °N. The two solid arrows indicate the southwestward subducted flow in the TNA and the northward AMOC return flow, respectively. The dashed arrow indicates the equatorward western boundary flow resulting from bifurcation of the subducted flow at the western boundary. Competition between this equatorward flow and the northward AMOC return flow is a key element of the subsurface oceanic gateway mechanism. (*Inset*) Shows the annual mean temperature at 30 m depth in the southern Caribbean and the location of VM12-107 (11.33 °N, 66.63 °W; 1,079 m), just outside the Cariaco Basin. Also shown are the locations of the Cariaco Basin and Laguna de Los Anteojos in northern Venezuela. The cooler temperatures near site VM12-107 are caused by coastal upwelling and are reflected in the calculated core-top Mg/Ca temperatures from this site. The temperature and salinity data are based on *World Ocean Atlas 2009* (24, 38).

during the late deglacial and early Holocene, *G. crassaformis* maintained a more constant depth habitat near the base of the thermocline (22, 23). Therefore, we chose to use *G. crassaformis* as a proxy for recording subsurface conditions within a constant depth range across the deglacial.

The *G. ruber* $\delta^{18}O$ record displays a glacial-interglacial difference of approximately 2.75‰, with the most positive values during the Last Glacial Maximum (LGM) (Fig. 2*A* and Table S1). In comparison, the *G. crassaformis* $\delta^{18}O$ record indicates a smaller glacial-interglacial amplitude of only approximately 1.2‰ (Fig. 2*B* and Table S2). Comparison of the $\delta^{18}O$ records shows a maximum $\Delta\delta^{18}O$ gradient between the mixed layer and the subthermocline over the last 7.2 ky. Because both temperature and salinity affect foraminiferal $\delta^{18}O$ values, this maximum Holocene $\Delta\delta^{18}O$ gradient suggests the vertical temperature/salinity gradient was reduced during the LGM and the deglacial.

Mg/Ca ratios in *G. ruber* were converted to upper mixed layer temperatures using an Atlantic core-top calibration (21) (Fig. 2*A*, see *SI Methods* and Fig. S4). Results indicate a core-top temperature of 25.7 °C, in agreement with the modern average annual temperature of 25.6 °C at 30 m water depth at the core site (24) (Figs. 1 and 2*C*). Because the core is located within an upwelling region, it is not surprising that cooler subsurface temperatures would have a greater influence on the average mixed layer temperature. The *G. ruber* Mg/Ca record indicates an LGM cooling of 4.5 °C. Mixed layer temperatures initially increase at 18 ky and warm to near modern values by 12.4 ky before abruptly cooling by 2.2 °C midway through the YD (Fig. 3*A*).

Because the abundance of *G. crassaformis* decreased through the Holocene, the youngest measured *G. crassaformis* Mg/Ca ratio is at 5.43 ky (Fig. 2*D*). Although conversion of Mg/Ca ratios in deep-dwelling planktonic foraminifera is not as well-calibrated as in *G. ruber*, the calculated Mg/Ca temperature for this interval is 10.0 °C. This temperature corresponds to modern conditions at 400 m in the Bonaire Basin (24) and is in agreement with ecological studies (20, 25). Unlike the *G. ruber* temperature record, the deglacial *G. crassaformis* Mg/Ca–temperature record indicates LGM subsurface temperatures that were slightly warmer than those in the early Holocene. Most surprising, the warmest

Table 1. Radiocarbon dates from VM12-107 based on mixed samples of *G. sacculifer* and *G. ruber* specimens

Depth (cm)	^{14}C Age	Age error (y)	Calendar age (ky)	Calendar age error (–) (ky)	Calendar age error (+) (ky)
2.5	1140	35	0.69	0.05	0.07
70.5	7900	55	8.37	0.13	0.13
82.5	9380	40	10.22	0.07	0.12
90.5	10050	65	11.05	0.26	0.14
104.5	10400	50	11.46	0.22	0.23
130.5	11200	50	12.67	0.10	0.16
160.5	12750	50	14.37	0.35	0.52
180.5	13450	60	15.74	0.56	0.64
220.5	15600	60	18.47	0.42	0.18
270.5	18500	90	21.59	0.26	0.47

Radiocarbon ages were converted to calendar ages using CALIB 6.0 (16), using the standard 400-y reservoir age correction.

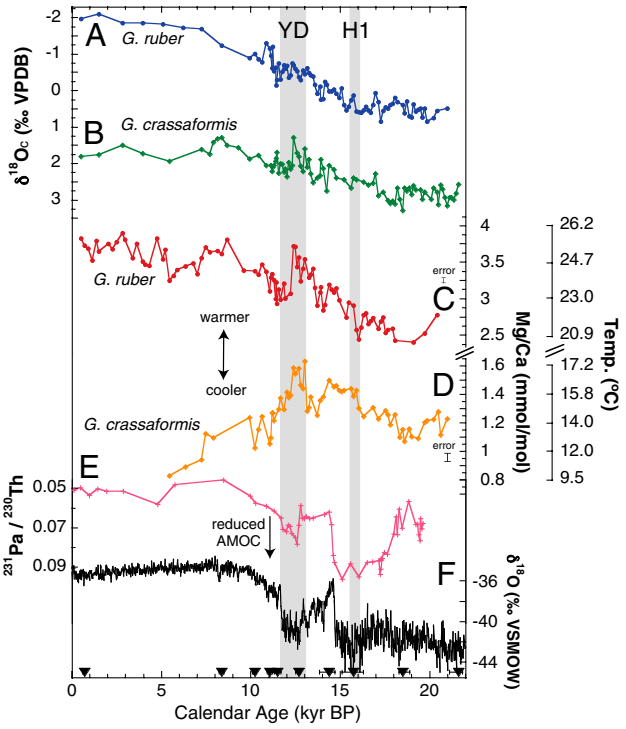

Fig. 2. Oxygen isotope and Mg/Ca records from site VM12-107 over the past 22 ky. Deglacial $\delta^{18}O$ and Mg/Ca ratio records in *G. ruber* (upper mixed layer) (*A*, *C*) and *G. crassaformis* (lower thermocline) (*B*, *D*) from southern Caribbean core VM12-107. The following equations were used to convert Mg/Ca ratios to temperature: for *G. ruber*, $Mg/Ca = 0.38\exp[0.09 * \text{Temp.}]$ (21), and for *G. crassaformis* $Mg/Ca = 0.339\exp[0.09 * \text{Temp.}]$ (21). Note the abrupt subsurface warming events during the YD and H1 in the *G. crassaformis* (orange line) temperature record. Analytical error on replicate Mg/Ca measurements on *G. ruber* and *G. crassaformis* are also shown (*C*, *D*). (*E*) Bermuda Rise $^{231}Pa/^{230}Th$ record (27) indicating changes in AMOC strength across the deglacial. (*F*) Greenland NGRIP ice core $\delta^{18}O$ record (26). Gray bars indicate the YD and H1. Black triangles on *x* axis show calibrated ^{14}C-based ages in VM12-107.

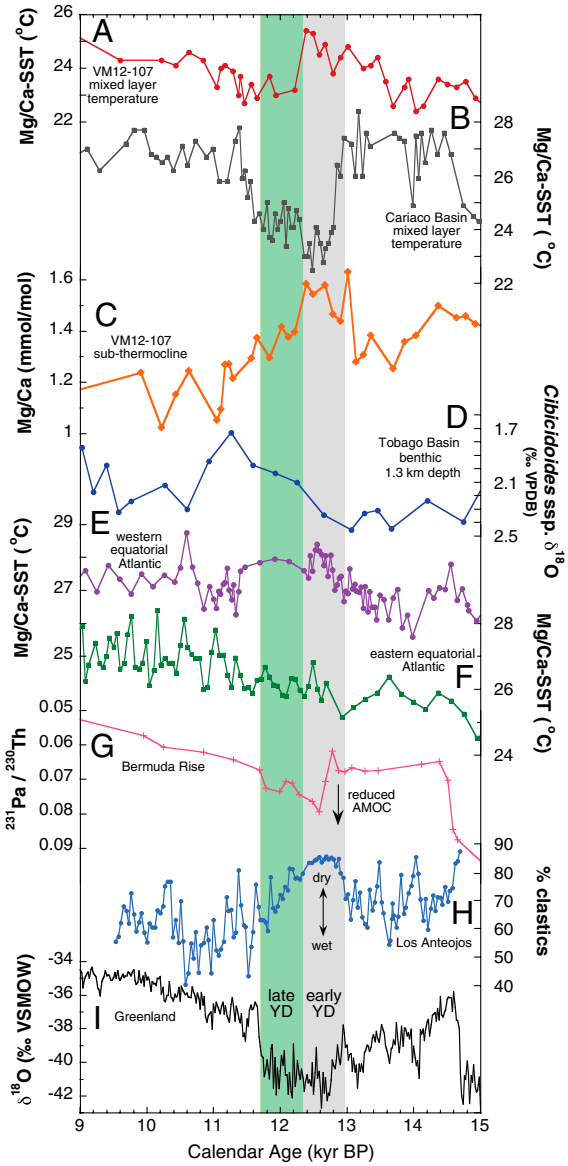

Fig. 3. Tropical Atlantic climate evolution across the YD. (*A*) The *G. ruber* Mg/Ca–temperature record from sediment core VM12-107. Note the early YD warming, followed by an abrupt cooling at 12.4 ky. (*B*) The *G. ruber* Mg/Ca–temperature record from the Cariaco Basin (10) showing an abrupt cooling at the onset of the YD. Note the coolest temperatures in the Cariaco Basin correspond to the warmest temperatures at our study site. (*C*) Mg/Ca ratios in *G. crassaformis* from VM12-107 indicating an abrupt subsurface warming in the Bonaire Basin at the start of the YD. (*D*) The ice volume-corrected Tobago Basin benthic foraminiferal $\delta^{18}O$ record (14), using an updated age model based on CALIB 6.0 (16), indicating a gradual warming at 1.3 km water depth across the YD. (*E*) The *G. ruber* Mg/Ca–SST record from the western equatorial Atlantic (36) indicating significant warming during the early YD. (*F*) An eastern equatorial Atlantic SST record (28) based on Mg/Ca ratios in *G. ruber*. (*G*) Bermuda Rise $^{231}Pa/^{230}Th$ record (27) indicating changes in AMOC strength across the deglacial. (*H*) The percentage of clastic sediments in a Venezuelan Andes lake core record indicating the development of extremely arid conditions during the early YD and a gradual return to wetter conditions during the late YD (29). (*I*) The Greenland NGRIP ice core $\delta^{18}O$ record, indicating the abrupt return to cold temperatures in Greenland during the YD (26). The gray and green bars indicate the early and late YD, respectively.

subsurface temperatures correspond to the early YD, when subsurface temperatures averaged 6.8 °C warmer (SD 0.5, $n = 6$) than Holocene values (Fig. 2*D*).

Discussion

Acknowledging there is debate about the Mg/Ca–temperature relationship in deep-dwelling planktonic foraminifera (21, 25), the *G. crassaformis* Mg/Ca ratios during the early YD show a 57% increase relative to Holocene ratios and an 18% increase at the start of the YD (Fig. 3*C*). This provides convincing evidence for an abrupt subsurface warming associated with the initiation of the YD at 13.01 ky (+0.24; −0.15 ky) that is within age model error of the start of the YD in the North Greenland Ice Core Project (NGRIP) ice core record at 12.896 ky (±0.138 ky) (26). Although not as well resolved, *G. crassaformis* Mg/Ca ratios also increase by 15% at approximately 16 ky, likely reflecting a subsurface warming associated with H1 as well (Fig. 2*D* and Fig. S5). It is not surprising that the magnitude of subsurface temperature change across H1 is not the same as during the YD, given that the boundary conditions and AMOC states bracketing these events were significantly different. Going into H1, AMOC was already in a weakened LGM state, and is thought to have decreased even further during the event (27) (Fig. 2*E*). In contrast, the period preceding the YD was characterized by a stronger AMOC state (27) (Fig. 2*E*). Thus, the greater subsurface temperature response at the start of the YD may reflect a larger magnitude of AMOC change. Additionally, AMOC remained in a significantly weakened state after H1 and into the "Mystery Interval" for approximately another 1,000 y before rapidly increasing at the Bølling-Allerød transition at 14.5 ky (27) (Fig. 2*E*). Therefore, we would not expect to find a subsurface cooling trend on the transition out of H1, as observed in our record at the termination of the YD.

A Tobago Basin benthic foraminiferal $\delta^{18}O$ record was interpreted to indicate intermediate-depth warming associated with AMOC slowdowns during the YD and H1 (14) (Figs. 3*D* and 4*A*). However, because benthic $\delta^{18}O$ values are affected by variations in water mass, salinity, and temperature, the cause of these $\delta^{18}O$ changes remains uncertain. Unlike the abrupt warming between 400–600 m at the onset of the YD suggested by the VM12-107 *G. crassaformis* Mg/Ca record (Fig. 3*C*), the Tobago Basin benthic $\delta^{18}O$ record suggests a much more gradual warming across the event at a depth of almost 1.3 km (Fig. 3*D*). In fact, most of the warming in the Tobago Basin record occurs during the late YD, a period characterized by subsurface cooling in the Bonaire Basin. Therefore, it is likely that different mechanisms were responsible for the temperature evolution at these two sites.

Changes in the $^{231}Pa/^{230}Th$ ratio recorded in sediments from the Bermuda Rise are thought to reflect AMOC variability across the last deglacial (27). As AMOC is reduced, the export of ^{231}Pa out of the Atlantic decreases, resulting in an increase in sediment $^{231}Pa/^{230}Th$ ratios (Fig. 3*G*). Because the estimated response time for this proxy is approximately 500 y (27), the $^{231}Pa/^{230}Th$ record will not reflect an abrupt change in AMOC. Therefore, the increase in Bermuda Rise $^{231}Pa/^{230}Th$ ratios at 12.7 ky is consistent with a major reduction in AMOC at the start of the YD at 12.896 ky (±0.138 ky) in the NGRIP ice core record (Fig. 3*I*), followed by a gradual strengthening of AMOC during the late YD. Comparison of the Bermuda Rise $^{231}Pa/^{230}Th$ record with our *G. crassaformis* Mg/Ca record suggests that subsurface temperatures in the southern Caribbean warmed as AMOC abruptly weakened at the start of the YD and that subsurface temperatures in the western tropical Atlantic gradually cooled as AMOC strengthend during the late YD.

The *G. ruber* temperature record from VM12-107 also indicates an increase in mixed layer temperatures during the first 600 y of the YD (Fig. 3*A*), consistent with previous temperature reconstructions from the western TNA (11–13, 28) (Figs. 3*E* and 4*A*). Remarkably, both the *G. ruber* and *G. crassaformis* Mg/Ca records indicate a cooling midway through the YD at 12.4 ky, well before the termination of the event in the Greenland ice core record (Fig. 3*I*), suggesting that subsurface temperatures

significantly influenced mixed layer conditions during this interval (Fig. 3*A* and *C*). As shown in a recent modeling study, subsurface warming associated with a reduction in AMOC can influence mixed layer temperatures in zones of strong coastal upwelling (8). Therefore, intensification of coastal upwelling in the TNA during the YD is predicted to increase mixed layer temperatures at sites along the western boundary current, as reflected in the VM12-107 *G. ruber* Mg/Ca–temperature record. In contrast, a well-resolved *G. ruber* Mg/Ca–temperature record from inside the Cariaco Basin indicated a large cooling of 4 °C at the start of the YD (10) (Fig. 3*B*). Because the Cariaco Basin's shallow sill (<100 m during the deglacial) would inhibit the inflow of warm subsurface waters characteristic of the open TNA, the significant surface cooling in the Cariaco Basin *G. ruber* Mg/Ca record is additional evidence that regional mixed layer temperatures were influenced by a strong subsurface warming. Unlike in the TNA, the mixed layer cooling inside the Cariaco Basin most likely reflects a combination of atmospheric-induced cooling and increased upwelling of cold intermediate waters restricted to inside the basin.

The Cariaco Basin *G. ruber* Mg/Ca–temperature record also indicates a two-phased YD, with the most intense cooling and strongest upwelling occurring during the first 600 y (Fig. 3*B*). Intensification of upwelling in the Cariaco Basin is consistent with a southward displacement of the intertropical convergence zone (ITCZ) and decreased rainfall over northern Venezuela. A recent sedimentological study of a Venezuelan lake core (29) also suggested the most arid conditions in the southern Caribbean occurred during the first 600 y of the YD (Fig. 3*H*). Together, these proxy reconstructions suggest the first half of the YD was most extreme, when regional aridity and upwelling were at a maximum.

To determine if the subsurface temperature increase identified in our proxy record during the YD is consistent with the previously identified mechanism found in an AOGCM water-hosing simulation conducted under present-day conditions (3), we analyze a new set of water-hosing simulations using LGM forcings and boundary conditions (30). Observational data show that warm salinity maximum waters (SMW) from the North Atlantic subtropical gyre are subducted and carried equatorward via the North Atlantic subtropical cell (STC). However, the modern equatorward pathway of the STC is blocked by strong northward AMOC return flow along the western boundary, resulting in a sharp subsurface temperature gradient separating the warm, salty subducted SMW from the fresher tropical gyre water (31–33) (Fig. 1). A recent modeling study showed that when AMOC and its northward return flow weaken, the maximum subsurface temperature gradient zone at the western boundary gives rise to a maximum subsurface warming (2). The warming responds quickly to the freshwater forcing because of a planetary wave-adjustment process (1, 3, 34). If the AMOC slowdown is sufficiently strong, causing its return flow to be weaker than the equatorward branch of the North Atlantic STC (dashed arrow in Fig. 1), the warm SMW can flow into the equatorial zone and subsequently into the tropical South Atlantic (2). Through upwelling, the subsurface warming can influence SSTs, affecting the position and strength of the ITCZ (3). However, this mechanism has only been identified in AOGCM experiments under modern climate conditions (3) and has not yet been tested for past abrupt climate events.

Analyses of LGM water-hosing simulations confirm the operation of the subsurface oceanic mechanism under LGM climate conditions (*SI Methods*, Figs. S6 and S7). Even with a relatively weak freshwater forcing (0.1 Sv), the simulation produces a substantial subsurface warming in the western TNA (Fig. 4*B* and Fig. S8). The averaged temperature between 300–600 m warmed by approximately 5 °C near the maximum subsurface temperature gradient zone (Fig. 4*B*). At the surface, the model simulation shows patches of surface warming off the northern South American coast (Fig. 4*A*) produced by coastal upwelling that brings the strong subsurface warming to the surface, counteracting the surface cooling induced by atmospheric processes (8). This finding supports our proxy reconstruction indicating that subsurface warming during the early YD significantly influenced mixed layer conditions in the Bonaire Basin, located within a upwelling zone (Fig. 3 *A* and *C*).

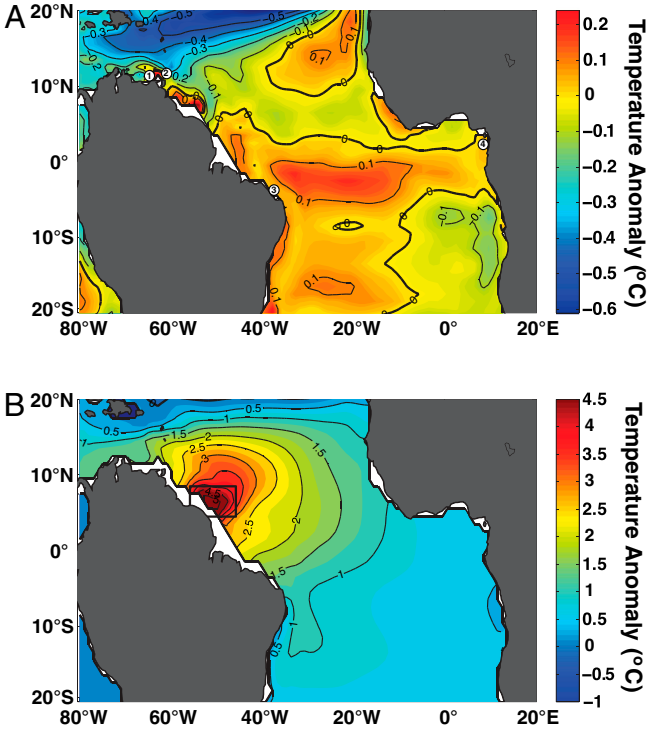

Fig. 4. Water-hosing simulation results under LGM forcings and boundary conditions. Changes in (*A*) surface (averaged between 5 and 35 m), and (*B*) subsurface (averaged between 300 and 600 m) temperatures between a LGM water-hosing and control simulation. The temperature change was computed as the difference between: (*i*) the average temperature of the last 20 y of the 100-y hosing run where a freshwater forcing of 0.1 Sv was held constant, and (*ii*) the average temperature of the same period of the control simulation. Time evolution of the subsurface temperature change averaged over the maximum subsurface temperature gradient zone indicated by the rectangle (*Lower*) is shown in Fig. S7. (*A*) Also shows the site locations (corresponding to encircled numbers) for: (*i*) VM12-107 in the Bonaire Basin, (*ii*) the Tobago Basin core M35003-4 (14), (*iii*) the western equatorial Atlantic core GeoB3129-3911 (28), and (*iv*) the eastern equatorial Atlantic core MD03-2707 (36).

Our new high-resolution paleotemperature reconstructions and modeling analyses provide evidence that abrupt changes in TNA climate were coupled to AMOC variability across the deglacial. The most likely explanation for the abrupt subsurface warming in the southern Caribbean at the start of the YD is a large change in horizontal heat advection near the maximum subsurface temperature gradient zone caused by weakening of the western boundary current in response to a sudden AMOC reduction. As the western boundary current continued to weaken and reach a threshold, warm SMW intruded into the equatorial zone along the western boundary and subsequently spread into the tropical South Atlantic, producing surface warming south of the equator (3). Previous SST reconstructions from the eastern tropical South Atlantic suggest a warming at the start of the YD (35, 36) (Figs. 3*F* and 4*A*), consistent with the subsurface oceanic gateway mechanism. Together with atmospheric-induced surface cooling in the TNA, this caused the ITCZ to shift to its most extreme southern position during the early YD. Then, the SMW gradually cooled because of atmospheric processes at their source region, and the subsurface warming diminished in the TNA during the late YD. This would cause SSTs in tropical upwelling zones to also cool, affecting the position and strength of the ITCZ during the second half of the YD, well before the termination of

the event in the Greenland ice core record (Fig. 3*I*). Therefore, the transition out of the YD may have started with a reorganization of the tropical hydrologic cycle. Although this mechanism most likely explains the subsurface warming associated with H1, the evolution of the subsurface temperature response across H1 is not the same as during the YD because of the differing AMOC states bracketing each event. This study provides evidence that subsurface temperature changes along the TNA western boundary current were a distinctive feature of AMOC-induced ocean circulation changes across the abrupt climate events of the last deglacial, forming a critical teleconnection between high- and low-latitude climate change.

Methods

To minimize intraspecific geochemical variations, specimens of *G. ruber* (white variety) and *G. crassaformis* were collected from the 250–350-μm and the 425–500-μm size fractions, respectively. Each *G. ruber* $\delta^{18}O$ analysis is based on 20 individuals, and each Mg/Ca measurement was made on at least 50 shells (run in duplicate). Because there is less seasonal variability in the thermocline and fewer deep-dwelling specimens, we used 4–6 individuals of *G. crassaformis* for each $\delta^{18}O$ analysis and 6–10 for trace metal analysis, whenever possible. Samples for stable isotope analysis were sonicated before analysis at Texas A&M University's Stable Isotope Geosciences Facility. Analytical uncertainty for our reported $\delta^{18}O$ measurements is better than 0.07‰. Samples for trace metal analysis were first sonicated in rinses of ultrapure water and methanol, cleaned in hot reducing and oxidizing solutions, and leached in dilute nitric acid. All clean work was conducted under trace metal clean conditions. Samples were then analyzed using isotope dilution on a High-Resolution Inductively Coupled Plasma Mass Spectrometer at Texas A&M University. A suite of trace and minor element measurements was made on each sample, including Ca, Mg, Sr, Na, Ba, U, Al, Mn, and Fe. The pooled SD on replicate Mg/Ca measurements for *G. ruber* was 2.3% (df = 86 based on 103 analyzed intervals), and for *G. crassaformis* was 3.92% (df = 52 based on 61 analyzed intervals). Analyses with either anomalously high (>100 μmol/mol) Al/Ca, Fe/Ca, or Mn/Ca ratios or low-percent recovery (<20%) were rejected. Analyses with high Al/Ca indicate the presence of detrital clays that were not removed during the cleaning process. Elevated levels of Fe/Ca or Mn/Ca indicate the presence of diagenetic coatings that were not removed during the cleaning process. Low-percent recovery values indicate the loss of shell material during the cleaning process, most likely caused by human error.

The Community Climate System Model, version 3.0, was used for the numerical simulations analyzed in this study. The model configuration is the standard intermediate-resolution (T42x1), consisting of: (*i*) the Community Atmosphere Model, version 3.0, coupled to the Community Land Model, version 3.0, with a triangular spectral truncation at 42 wavenumbers (roughly 2.8° in longitude and latitude); and (*ii*) the Parallel Ocean Program, version 1.4.3, coupled to the Community Sea Ice Model, version 5.0, at 1° horizontal resolution (37).

ACKNOWLEDGMENTS. We thank A. Gondran for assistance with geochemical analyses and the Lamont Doherty Earth Observatory core repository for sediment core material. This project was funded by National Science Foundation Grant OCE-1102743 (to M.S. and P.C.) and by National Oceanic and Atmospheric Adminstration Grant NA11OAR4310154 (to P.C.). P.C. also acknowledges support from the National Science Foundation of China (Grants 41028005, 40921004, and 40930844) and the Chinese Ministry of Education's 111 project (Grant B07036).

1. Zhang R (2007) Anticorrelated multidecadal variations between surface and subsurface tropical North Atlantic. *Geophys Res Lett* 34:1–6.
2. Zhang R, Delworth TL, Held IM (2007) Can the Atlantic Ocean drive the observed multidecadal variability in Northern Hemisphere mean temperature? *Geophys Res Lett* 34:1–6.
3. Chang P, et al. (2008) Oceanic link between abrupt changes in the North Atlantic Ocean and the African monsoon. *Nat Geosci* 1:444–448.
4. Otto-Bliesner BL, Brady EC (2010) The sensitivity of the climate response to the magnitude and location of freshwater forcing: Last glacial maximum experiments. *Quat Sci Rev* 29:56–73.
5. Wen CH, Chang P, Saravanan R (2010) Effect of Atlantic meridional overturning circulation changes on tropical Atlantic sea surface temperature variability: A 2 1/2-layer reduced-gravity ocean model study. *J Clim* 23:312–332.
6. Cheng W, Bitz CM, Chiang JCH (2007) Adjustment of the global climate to an abrupt slowdown of the Atlantic meridional overturning circulation. *Past and Future changes of the Ocean's Meridional Overturning Circulation: Mechanisms and Impacts*, eds A Schmittner, JCH Chiang, and SR Hemming (AGU Monograph, Washington, DC), Vol 173, pp 295–314.
7. Chiang JCH, Cheng W, Bitz CM (2008) Fast teleconnections to the tropical Atlantic sector from Atlantic thermohaline adjustment. *Geophys Res Lett* 35:1–5.
8. Wan XQ, Chang P, Saravanan R, Zhang R, Schmidt MW (2009) On the interpretation of Caribbean paleo-temperature reconstructions during the Younger Dryas. *Geophys Res Lett* 36:1–6.
9. Guilderson TP, Fairbanks RG, Rubenstone JL (2001) Tropical Atlantic coral oxygen isotopes: Glacial-interglacial sea surface temperatures and climate change. *Mar Geol* 172:75–89.
10. Lea DW, Pak DK, Peterson LC, Hughen KA (2003) Synchroneity of tropical high latitude Atlantic temperatures over the last glacial termination. *Science* 301:1361–1364.
11. Rühlemann C, Mulitza S, Muller PJ, Wefer G, Zahn R (1999) Warming of the tropical Atlantic ocean and slowdown of thermohaline circulation during the last deglaciation. *Nature* 402:511–514.
12. Hüls M, Zahn R (2000) Millennial-scale sea surface temperature variability in the western tropical North Atlantic from planktonic foraminiferal census counts. *Paleoceanography* 15:659–678.
13. Schmidt MW, Spero HJ, Lea DW (2004) Links between salinity variation in the Caribbean and North Atlantic thermohaline circulation. *Nature* 428:160–163.
14. Rühlemann C, et al. (2004) Intermediate depth warming in the tropical Atlantic related to weakened thermohaline circulation: Combining paleoclimate data and modeling results for the last deglaciation. *Paleoceanography* 19:1–10.
15. Came R, et al. (2007) North Atlantic intermediate depth variability during the Younger Dryas: Evidence from benthic foraminiferal Mg/Ca and the GFDL R30 coupled climate model. *Past and Future Changes in the Ocean's Overturning Circulation: Mechanisms and Impacts on Climate and Ecosystems*, eds A Schmittner, JCH Chiang, and SR Hemming (American Geophysical Union, Washington, DC).
16. Stuiver M, Reimer PJ, Reimer R (2011) *CALIB Radiocarbon Calibration* (Queen's University, Belfast, Ireland), Version 60.
17. Hua Q, et al. (2009) Atmospheric ^{14}C variations derived from tree rings during the early Younger Dryas. *Quat Sci Rev* 28:2982–2990.
18. Southon J, Noronha AL, Cheng H, Edwards RL, Wang Y (2012) A high-resolution record of atmospheric ^{14}C based on Hulu Cave speleothem H82. *Quat Sci Rev* 33:32–41.
19. Muscheler R, et al. (2008) Tree rings and ice cores reveal C-14 calibration uncertainties during the Younger Dryas. *Nat Geosci* 1:263–267.
20. Steph S, Regenberg M, Tiedemann R, Mulitza S, Nürnberg D (2009) Stable isotopes of planktonic foraminifera from tropical Atlantic/Caribbean core-tops: Implications for reconstructing upper ocean stratification. *Mar Micropaleontol* 71:1–19.
21. Anand P, Elderfield H, Conte MH (2003) Calibration of Mg/Ca thermometry in planktonic foraminifera from a sediment trap time series. *Paleoceanography* 18:1–15.
22. Cléroux C, Lynch-Stieglitz J, Schmidt MW, Cortijo E, Duplessy JC (2009) Evidence for calcification depth change of *Globorotalia truncatulinoides* between deglaciation and Holocene in the Western Atlantic Ocean. *Mar Micropaleontol* 73:57–61.
23. Cléroux C, Lynch-Stieglitz J (2010) What caused *G.truncatulinoides* to calcify in shallower water during the early Holocene in the western Atlantic/Gulf of Mexico? *PAGES First Young Scientist Meeting* (IOP Conference Series: EES, Philadelphia).
24. Antonov JI, et al. (2006) World ocean atlas 2005. *NOAA Atlas NESDIS 6* (USGPO, Washington, DC) p 182.
25. Regenberg M, Steph S, Nürnberg D, Tiedemann R, Garbe-Schönberg D (2009) Calibrating Mg/Ca ratios of multiple planktonic foraminiferal species with delta O-18-calcification temperatures: Paleothermometry for the upper water column. *Earth Planet Sci Lett* 278:324–336.
26. Rasmussen SO, et al. (2006) A new Greenland ice core chronology for the last glacial termination. *J Geophys Res [Atmos]* 111:1–16.
27. McManus JF, Francois R, Gherardi J-M, Keigwin LD, Brown-Leger S (2004) Collapse and rapid resumption of Atlantic meridional circulation linked to deglacial climate changes. *Nature* 428:834–837.
28. Weldeab S, Schneider RR, Kölling M (2006) Deglacial sea surface temperature and salinity increase in the western tropical Atlantic in synchrony with high latitude climate instabilities. *Earth Planet Sci Lett* 241:699–706.
29. Stansell ND, et al. (2010) Abrupt Younger Dryas cooling in the northern tropics recorded in lake sediments from the Venezuelan Andes. *Earth Planet Sci Lett* 293:154–163.
30. Liu Z, et al. (2009) Transient simulation of last deglaciation with a new mechanism for Bolling-Allerod warming. *Science* 325:310–314.
31. Fratantoni DM, Johns WE, Townsend TL, Hurlburt HE (2000) Low-latitude circulation and mass transport pathways in a model of the tropical Atlantic ocean. *J Phys Oceanogr* 30:1944–1966.
32. Jochum M, Malanotte-Rizzoli P (2001) Influence of the meridional overturning circulation on tropical-subtropical pathways. *J Phys Oceanogr* 31:1313–1323.
33. Hazeleger W, Drijfhout S (2006) Subtropical cells and meridional overturning circulation pathways in the tropical Atlantic. *J Geophys Res [Oceans]* 111:1–13.
34. Kawase M (1987) Establishment of deep ocean circulation driven by deep-water production. *J Phys Oceanogr* 17:2297–2317.
35. Mulitza S, Rühlemann C (2000) African monsoonal precipitation modulated by interhemispheric temperature gradients. *Quat Res* 53:270–274.
36. Weldeab S, Lea DW, Schneider RR, Andersen N (2007) 155,000 years of West African monsoon and ocean thermal evolution. *Science* 316:1303–1307.
37. Collins WD, et al. (2006) The community climate cystem model, version 3 (CCSM3). *J Clim* 19:2122–2143.
38. Locarnini RA, et al. (2006) *World Ocean Atlas 2005*, (USGPO, Washington, DC), Temperature, Vol 1, p 182.